TRANSPORT PROPERTIES OF POROUS γ-ALUMINA FROM DIFFUSION IN LIQUIDS AND GASES

Petr UCHYTIL and Petr SCHNEIDER

Institute of Chemical Process Fundamentals,
Czechoslovak Academy of Sciences, 165 02 Prague 6-Suchdol

Received November 16th, 1987
Accepted November 23th, 1987

Transport characteristics of four porous samples with bidisperse or broad monodisperse pore structure were determined by combination of diffusion and permeation measurements with simple gases and compared with results obtained from diffusion of toluene or α,α,α-trifluorotoluene in cyclohexane in liquid phase. From comparison of both types of results it followed that all pores are decisive for the rate of diffusional transport in liquids, whereas only the wide transport pores are significant in gas diffusion.

Rates of many chemical processes (heterogeneous catalytic and noncatalytic reactions, adsorption etc.) can be significantly affected by mass transport in porous media. For characterization and prediction of this transport it is necessary to replace the real porous structure by a simple model; parameters of the model are, then, material constants of the porous solid and are independent of the conditions at which the process takes place. One of such models is the mean-transport pore model (MTPM)[1]. In MTPM it is assumed that the mass transport takes place only in some pores which are present in the porous solid (transport pores); transport-pores are modeled as a bundle of parallel cylindrical capillaries with mean radius $\langle r \rangle$ (mean transport-pore radius). The width of the distribution of transport-pore radii is characterized by the mean of squared transport-pore radii $\langle r^2 \rangle$. Porosity of transport pores, ε_t, which must be less or equal to the total porosity ε ($\varepsilon_t \leqq \varepsilon$), appears in the MTPM expressions always in combination with the tortuosity of transport pores, q_t, in the form of a geometric parameter ψ ($\psi = \varepsilon_t/q_t$).

It was the aim of this contribution to verify whether measurements with gases and liquids give the same transport parameters and/or whether it would be feasible to combine such results. Such a combination was attempted earlier by Riekert et al.[2] who tried to predict the effective diffusion coefficient of carbon monoxide in impregnated $CuO/\gamma\text{-}Al_2O_3$ catalyst from results of independent pure diffusion measurements in gas and liquid phases. The predicted effective diffusivity was compared with the value obtained through evaluation of diffusion retardation of catalytic gas phase oxidation of carbon monoxide. The threefold difference was ascribed

by the authors to the nonhomogeneous distribution of active component on catalyst carrier, which influences the local reaction rates and, thus, the mass transfer rate.

In this paper we have evaluated transport parameters of a series of texturally differing γ-Al_2O_3 samples from the combination of diffusion and permeation measurements in gas phase and compared them with results of diffusion measurements of toluene and α,α,α-trifluorotoluene in cyclohexane in liquid phase.

EXPERIMENTAL

Pellets. Cylindrical pellets of γ-Al_2O_3 (diameter × height = 5 mm × 5 mm) with bidisperse pore structure were prepared from powdered aluminium hydroxide with addition of 4 wt. % aluminium stearate in a laboratory press with improved control of compression pressure at three pressure levels. Distributions of pore volumes were determined by mercury porosimetry (porosimeter AutoPore 9200, Micromeritics, U.S.A.) on samples calcinated in air (550°C, 5 hours). Measurements were also carried out on cylindrical pellets (diameter × height = = 5·4 mm × 3·6 mm) of an industrial catalyst ICI 52-1 (Imperial Chemicals Industries, England) with broad monodisperse pore structure.

Permeation of gases. For permeation measurements of four nonadsorbing gases (hydrogen, helium, nitrogen, argon) at laboratory temperature the permeation cell described by Fott and Petrini[3] was employed. Effective permeability coefficients, B, were evaluated from the time change of a small pressure difference between two cell parts, separated by a metallic partition with cylindrical holes in which the porous pellets were fastened. Effective permeability coefficients were determined in the pressure interval 0·7—40 kPa and at laboratory temperature.

Binary counter-current gas diffusion. The diffusion cell which utilizes the validity of Graham's law was described earlier[4]. Measurements were made with four gas pairs: hydrogen–nitrogen, hydrogen–argon, helium–nitrogen, and helium–argon, at laboratory temperature and pressure.

Liquid phase diffusion. Porous pellets (usually 16 pieces) were placed in 15 small closed glass vials (the difference between pellets weight in individual vials was less than 0·5% of the mean) and cyclohexane was added so that all pellets were immersed (approximately 3 cm^3; the difference between cyclohexane amounts in the vials was less than 0·3% of the mean). Because of the low amount of cyclohexane the concentration changes of diffusing component during the diffusion runs are amplified which makes the analysis more precise. At time $t = 0$ 25 μl of toluene or α,α,α-trifluorotoluene was added into each vial. Initial toluene concentration was approximately 0·15 mmol/cm^3 (i.e. 1·6 mole %); for α,α,α-trifluorotoluene these values were 0·1 mmol/cm^3 (1·1 mole %). The vials were vigorously shaken and after different times for each vial the measurement was stopped by removing the liquid for analysis. The last samples were taken after 3 and 5 hours; because concentration of the diffusing components were identical these values were used as equilibrium concentrations c_A^∞. All measurements were made at 18—24°C.

Equilibrium adsorption isotherms of toluene and α,α,α-trifluorotoluene were determined in the following way: solutions of toluene or α,α,α-trifluorotoluene in cyclohexane of different concentrations were added always into five vials (volume approximately 10 cm^3) filled with porous pellets; the highest concentrations in equilibrium runs corresponded to initial concentrations in diffusion runs. After attainment of adsorption equilibrium (about 48 hours) liquid samples were withdrawn from the vials for analysis.

Toluene–cyclohexane mixtures were analysed by refractometry (differential refractometer R 401, Waters, U.S.A.; refractive indices at 20°C (ref.[5]): n_D(cyclohexane) = 1·4262, n_D(toluene) =

= 1·4969). The relative error of toluene concentration determination was estimated at 3%. Densitometry was used for analysis of α,α,α-trifluorotoluene–cyclohexane mixtures (densitometer DMA 60 + 602, A. Paar, Austria; densities at 20°C (ref.[5]): d(α,α,α-trifluorotoluene) = 1·1886 g/cm^3, d(cyclohexane) = 0·7792 g/cm^3). Calibration was carried out with redistilled water and cyclohexane; accuracy of density determinations was about $2 \cdot 10^5$ g/cm^3 which corresponds to 2—3% error in concentration.

RESULTS AND DISCUSSION

Textural properties of porous pellets are summarized in Table I. Pore volume distributions are presented in Fig. 1. It can be seen that all γ-Al_2O_3 samples have a bidisperse pore structure and the total pore volume and macropore size decrease with increase in compacting pressure. At the same time the mesopore size is not affected by the compacting process. As a result of the similarly of mesopore sizes and volumes, the specific surface areas of samples differ only slightly. The ICI 52-1 pellets were monodisperse with mesopore radii around 5·9 nm.

Permeation of gases. The effective permeability coefficient, B, is defined by Eq. (*1*)

$$N = -B(\mathrm{d}c/\mathrm{d}x), \qquad (1)$$

where N is the molar permeation flux density (mol cm^{-2} s^{-1}), c the total molar gas concentration ($c = p/RT$; p gas pressure, T temperature (K), R gas constant) and x the geometric coordinate in the direction of permeation. Pressure dependence of this

TABLE I
Textural characteristics of porous samples

Sample	Compacting pressure MPa	Density[a] g/cm^3		Porosity[b] %		Specific surface[c] m^2/g	Most frequent pore radii, nm	
		ϱ	ϱ_p	ε	ε_{ma}		meso	macro
γ-Al_2O_3	100	3·255	0·80	0·75	0·31	236	2·5	270
γ-Al_2O_3	150	3·270	0·90	0·72	0·22	217	3·0	180
γ-Al_2O_3	250	3·288	1·05	0·68	0·14	210	3·0	100
ICI 52-1	—	4·146	1·50	0·64	0·02	98	5·9	—

[a] True (skeletal) density, ϱ: pycnometrically with helium (AutoPycnometer 1320, Micromeritics, U.S.A.); apparent density, ϱ_p: pycnometrically with mercury (AutoPore 9200, Micromeritics, U.S.A.; [b] total porosity $\varepsilon = 1 - (\varrho_p/\varrho)$; porosity of macropores, ε_{ma}, from pore size distribution; [c] BET (DigiSorb 2600, Micromeritics, U.S.A.).

coefficient is expressed by the modified Weber equation (cf. ref.[1])

$$B = \langle r \rangle \psi K[(\omega + \mathscr{K})/(1 + \mathscr{K})] + \langle r^2 \rangle \psi(p/8\mu), \qquad (2)$$

where $\langle r \rangle$ is the mean transport-pore radius, $\langle r^2 \rangle$ the mean of squared transport-pore radii, ψ the geometric parameter of MTPM, ω a numerical coefficient, $\mathscr{K}$ the Knudsen number (ratio of molecular mean free path, λ, and pore diameter: $\mathscr{K} = \lambda/2\langle r \rangle$), μ gas viscosity and K the Knudsen coefficient

$$K = (2/3)\sqrt{(8RT/\pi M)} \qquad (3)$$

(M is the gas molecular weight). On using kinetic theory of gases Eq. (2) can be rewriten as[1]

$$B/K = \langle r \rangle \psi[(\omega + \mathscr{K})/(1 + \mathscr{K})] + \langle r^2 \rangle \psi(3\pi/64)(1/\lambda). \qquad (4)$$

According to Eq. (4), the permeabilities of different gases in the same porous sample must fall on the same line when plotted in coordinates B/K versus $1/\lambda$; from this line it is possible to evaluate the products of transport parameters $\langle r \rangle \psi$ and $\langle r^2 \rangle \psi$.

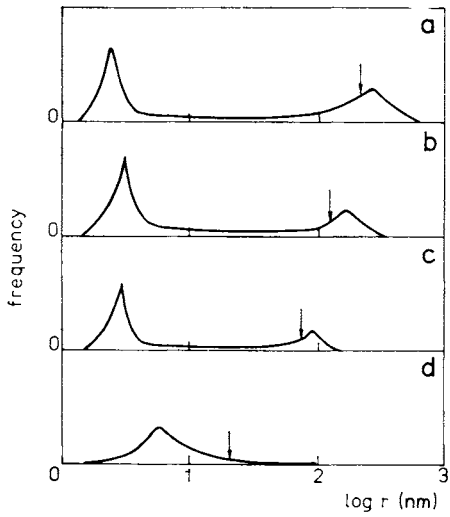

FIG. 1

Pore size distributions of porous samples γ-Al_2O_3: compacting pressure (MPa): a 100, b 150, c 250, d ICI 52-1. Arrows show $\langle r \rangle$*

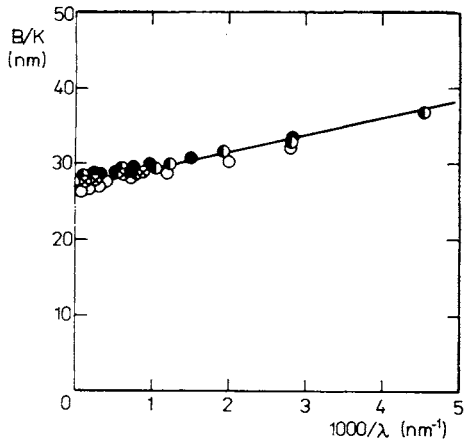

FIG. 2

B/K versus $1/\lambda$ for γ-Al_2O_3 compacted at 100 MPa. ○ Hydrogen, ⊗ helium, ◐ nitrogen, ● argon

Fig. 2 illustrates this dependence for the γ-Al_2O_3 sample compacted at 100 MPa; analogous straight lines were obtained also for other samples (molecular mean free path lengths, λ, were taken from the literature[6]). Obviously, the numerical coefficient ω from Eqs (*2*) and (*4*) is $\omega = 1$, which simplifies Eqs (*2*) and (*4*) to straight line dependences. Transport parameters $\langle r \rangle \psi$ and $\langle r^2 \rangle \psi$ can, then, be obtained by linear least squares method. The obtained parameters, together with 95% confidence intervals, are summarized in Table II. From the size of confidence intervals it follows that the accuracy of determination of transport parameter products is very satisfactory.

Gas diffusion. According to MTPM, the diffusion flux of gas A in the binary A–B can be expressed as[4]

$$N_A = (-c\, dy_A/dx)\{[(1 - \alpha_{AB} y_A)/\psi \mathscr{D}_{AB}] + (1/\langle r \rangle \psi K_A)\}^{-1}, \qquad (5)$$

where y_A is the mole fraction of component A, $\mathscr{D}^m_{AB}$ is the binary bulk diffusion coefficient of gas pair A–B and α_{AB} is defined as

$$\alpha_{AB} = 1 - \sqrt{(M_A/M_B)}\,. \qquad (6)$$

The differential equation (*5*) is supplemented by boundary conditions which express that in the experimental arrangement pure gases A and B are present at the pellet faces:

$$x = 0, \quad y_A = 1$$

$$x = L, \quad y_A = 0.$$

TABLE II

Transport parameters from measurements with gases

Sample	Compacting pressure MPa	Permeation		Diffusion		Combination	
		$[\langle r \rangle \psi]_{perm}$ nm	$\langle r^2 \rangle \psi$ nm^2	$\langle r \rangle_{dif}$ nm	ψ_{dif} —	$\langle r \rangle^*$ nm	ψ^* —
γ-Al_2O_3	100	27·05 ± 0·4	15·36 ± 0·2	148	0·14	235	0·12
γ-Al_2O_3	150	12·15 ± 0·2	5·56 ± 0·1	50	0·17	125	0·10
γ-Al_2O_3	250	5·96 ± 0·1	1·72 ± 0·1	—	—	80	0·07
ICI 52-1[a]	—	1·90 ± 0·05	0·15 ± 0·06	60	0·04	22	0·09

[a] According to Fott et al.[1]

Expression for the total molar diffusion flux density, N ($N = N_A + N_B$), can be obtained by integration of Eq. (5) with the above boundary conditions:

$$N = \psi(c/L)\,\mathscr{D}^{m}_{AB} \ln \{[(\mathscr{D}^{m}_{AB}/\langle r\rangle K_A) + 1]/[(\mathscr{D}^{m}_{AB}/\langle r\rangle K_A) + 1 - \alpha_{AB}]\} . \quad (7)$$

Transport parameters ψ and $\langle r\rangle$ which appear in Eq. (7) can be evaluated from experimental data by minimization of the sum of the squared deviations between experimental and calculated total molar diffusion flux densities for all gas pairs used (Q). Because ψ appears in Eq. (7) linearly the determination of optimum parameter pair $\langle r\rangle_{dif}$, ψ_{dif} is greatly simplified. Optimum parameters determined in this way are summarized in Table II (the necessary binary bulk diffusivities $\mathscr{D}^{m}_{AB}$ were taken from the literature[7]). The reliability of these parameter is, however, not very high as they are based on experimental data for four gas pairs only. This is clealry demonstrated in Fig. 3 where the 95% confidence region is shown for one γ-Al_2O_3 sample.

Transport parameters from combination of measurements with gases. The high reliability of parameter products $[\langle r\rangle\,\psi]_{perm}$ from permeation can be utilized for determination of individual optimum parameters $\langle r\rangle^*$, ψ^* which can give a true picture of experimental permeation and diffusion results for gases simultanously.

Parameters $\langle r\rangle^*$ and ψ^* can be determined by simultaneous minimization of the sum of squared deviations of total diffusion flux densities for the four gas pairs employed (Q) under the constraint that their product is equal to $[\langle r\rangle\,\psi]_{perm}$ from permeation. This procedure is graphically illustrated in Fig. 3, where curve *2* corresponds to the condition $\langle r\rangle\,\psi = [\langle r\rangle\,\psi]_{perm}$. Part of curve *2* inside the 95% confidence region of diffusion results (**AB** in Fig. 3) demarcates combinations of parameters $\langle r\rangle$ and ψ which are statistically indistinguishable from the optimum pair for diffusion ($\langle r\rangle_{dif}$, ψ_{dif}) and at the same time are optimum for permeation because their product equals $[\langle r\rangle\,\psi]_{perm}$. Then the pair of optimum combined parameters $\langle r\rangle^*$, ψ^* is located on line *3* which is the locus of parameter combinations with lowest Q for given radius $\langle r\rangle$. Pairs $\langle r\rangle^*$, ψ^* for all studied porous samples are presented in Table II.

As the optimum mean transport-pore radii $\langle r\rangle^*$ for all γ-Al_2O_3 are located near the maxima for macropores on pore size distribution curves (cf. Fig. 1) it is obvious that the predominant part of the combined gas transport takes place in macropores. For monodisperse sample ICI 52-1 this radius corresponds to the widest mesopores for which there is no matching maximum on pore size distribution.

Liquid phase adsorption. It follows from the equilibrium adsorption measurements of toluene and α,α,α-trifluorotoluene in cyclohexane in porous samples that toluene is not adsorbed whereas with α,α,α-trifluorotoluene a weak adsorption takes place. Fig. 4 illustrates the adsorption data for γ-Al_2O_3 compacted at 250 MPa and the

ICI 52-1 sample which represent the extreme cases. Equilibrium adsorption of α,α,α--trifluorotoluene on all samples can be described by linear adsorption isotherms with equilibrium adsorption constants, K_{ads}, defined as

$$K_{ads} = q_A^+/c_A^+ , \qquad (8)$$

where q_A^+ and c_A^+ are the adsorbed amount per unit pore volume and concentration in liquid inside the pores at equilibrium, respectively. Equilibrium adsorption constants for γ-Al_2O_3 samples are similar: for samples compacted at 100, 150, and 250 MPa, K_{ads} = 1·9, 2·1, and 2·4, respectively. For ICI 52-1 K_{ads} = 0·7 was found

Diffusion in liquid phase. If the contribution of surface transport is disregarded,

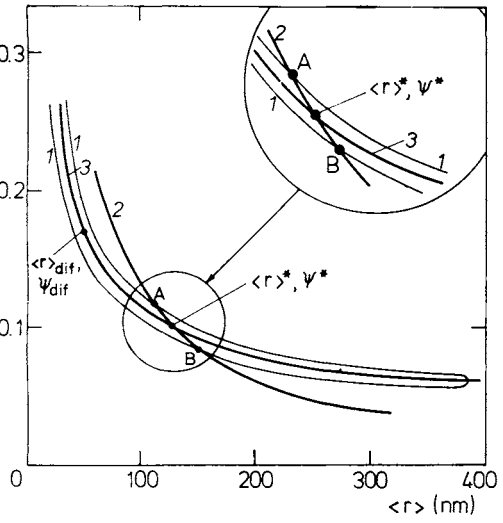

FIG. 3

Combination of gas phase measurements for γ-Al_2O_3 compacted at 150 MPa. *1* 95% Confidence region for parameters from diffusion measurements; *2* dependence $\psi = [\langle r\rangle \psi]_{perm}/\langle r\rangle$ from permeation measurements; *3* locus of optimum parameters ψ for given radius $\langle r\rangle$ for diffusion measurements; $\langle r\rangle_{dif}$, ψ_{dif}: optimum parameter pair for diffusion; $\langle r\rangle^*$, ψ^* optimum parameter pair from combination of diffusion and permeation measurements

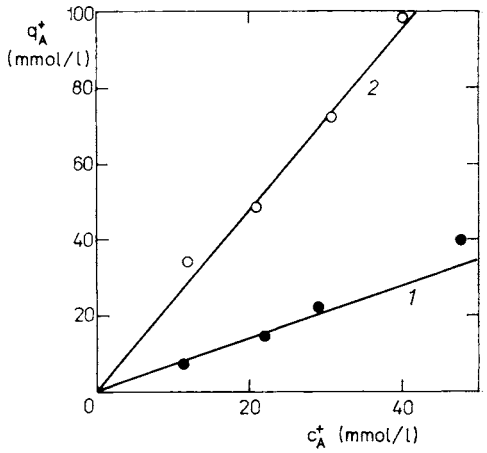

FIG. 4

Adsorption equilibrium of α,α,α-trifluorotoluene *1* ICI 52-1; *2* γ-Al_2O_3/250 MPa

diffusion of component A in liquid binary A–B can be described by the Fick's law

$$N_A = -D_{AB}(dc_A/dx), \tag{9}$$

where N_A is the molar diffusion flux density of component A (mol cm^{-2} s^{-1}), c_A its molar concentration, x the geometric coordinate in the direction of diffusion transport and D_{AB} the effective diffusion coefficient of A in binary A–B. This coefficient is related to the binary bulk liquid diffusivity of pair A–B, $\mathscr{D}_{AB}$, through the relation

$$D_{AB} = \psi_{liq}\mathscr{D}_{AB}. \tag{10}$$

For diffusing molecules which are small in comparison with the pore diameter, ψ_{liq} represents a geometric parameter which includes porosity and tortuosity of pores which are engaged in liquid diffusion transport.

The mass balance of component A when unsteady diffusion takes place in a spherical porous particle with radius R has the form

$$(\partial N_A/\partial r) + (2/r)N_A = \varepsilon\partial(c_A + q_A)/\partial t, \tag{11}$$

where q_A is the adsorbed amount of component A, referred to unit pore volume and r is the geometric coordinate in the spherical particle ($r = 0$ at the centre, $r = R$ at the outer surface). If adsorption is rapid in comparison to diffusion and the adsorption isotherm is linear, the adsorbed amount q_A can be expressed from the condition of adsorption equilibrium (*8*). Mass balance (*11*) can be then written as

$$D_{AB}[(\partial^2 c_A/\partial r^2) + (2/r)(\partial c_A/\partial r)] = \varepsilon(1 + K_{ads})(\partial c_A/\partial t). \tag{12}$$

Disappearance of component A from the bulk solution which surrounds the pellets is described by

$$V_L(\partial c_L/\partial t) = -(3W/R\varrho_p)\, D_{AB}(\partial c_A/\partial r)_{r=R} \tag{13}$$

(c_L is the concentration of A in the bulk solution of volume V_L and W is the weight of porous particles with apparent density ϱ_p) with boundary and initial conditions

$$(\partial c_A/\partial r)_{r=0} = 0\,; \quad (c_A)_{r=R} = c_L \tag{14}$$

$$c_L(t = 0) = c_L^\circ\,; \quad c_A(t = 0) = 0. \tag{15}$$

After attainment of the adsorption equilibrium

$$c_L = c_A = c_A^\infty. \tag{16}$$

Solution of the equation system (*12*)–(*16*) is given by Crank[8] in the form

$$[c_o^L - c_A(t)]/[c_o^L - c_A^\infty] = 1 - \sum_{n=1}^{\infty} \frac{6\alpha(\alpha + 1)}{9 + 9\alpha + a_n^2\alpha^2} \exp(-t/\tau), \qquad (17)$$

where

$$\alpha = v\varrho_p/[\varepsilon(1 + K_{ads})] \qquad (18)$$

$$\tau = R^2\varepsilon(1 + K_{ads})/(a_n^2 D_{AB}) \qquad (19)$$

and v is the volume of bulk solution per unit weight of the porous pellets ($v = V_L/W$), a_n are the roots of equation

$$\tan a_n = 3a_n/(3 + a_n^2\alpha) \quad n = 1, 2, \ldots, \qquad (20)$$

left-hand side of Eq. (*17*) gives the amount of component A which has diffused into the particle up to time t, referred to the pellet capacity $[M(t)/M(\infty) = (c_o^L - c_A(t))/(c_o^L - c_A^\infty)]$.

Effective diffusivities D_{AB} were determined from the experimental dependences $M(t)/M(\infty)$ versus t by minimization of the squared deviations between experimental and calculated results (in the calculations the cyclindrical porous pellets were replaced by equivalent spheres with the same geometric surface to volume ratio). The obtained values are summarized in Table III; the agreement of calculation with experiment is illustrated in Fig. 5 which also shows the accuracy of determination of D_{AB}. With α,α,α-trifluorotoluene the error in D_{AB} was estimated to 20% because the runs were repeated only twice.

TABLE III

Diffusion in liquid phase (cyclohexane solutions)

Sample	Compacting pressure MPa	Toluene		α,α,α-Trifluorotoluene	
		$D_{AB} \cdot 10^6$ cm²/s	ψ_{liq} —	$D_{AB} \cdot 10^6$ cm²/s	ψ_{liq} —
γ-Al_2O_3	100	6·0 ± 0·6	0·40 ± 0·04	4·0	0·36
γ-Al_2O_3	150	5·0 ± 0·6	0·33 ± 0·04	4·2	0·38
γ-Al_2O_3	250	4·2 ± 0·5	0·28 ± 0·03	5·0	0·45
ICI 52-1	—	—	—	5·0	0·45

The geometric parameters ψ_{liq} were determined from D_{AB} according to Eq. (*10*); for binary diffusivity in the system toluene–cyclohexane the experimental value[9] $\mathscr{D}_{AB}(20°) = 1{\cdot}5 \,.\, 10^{-5}$ cm^2/s was used. Diffusivity in the binary α,α,α-trifluorotoluene–cyclohexane was estimated[10]: $\mathscr{D}_{AB} = 1{\cdot}1 \,.\, 10^{-5}$ cm^2/s. The obtained parameters ψ_{liq} are given in Table III. Taking into account the limited accuracy of D_{AB} and $\mathscr{D}_{AB}$, the agreement of parameters ψ_{liq} for different porous pellets determined from diffusion in both binaries can be considered as adequate.

Comparison of transport parameters from measurements in liquid and gas phase. If the MTPM would describe correctly the situation by both gas and liquid transport then the geometric parameters ψ^* suitable for gas transport description should agree with parameters ψ_{liq} which comport with liquid diffusion. Comparison of ψ^* and ψ_{liq} from Tables II and III, however, shows that ψ_{liq} are three to four times larger than ψ^*.

The probable reason is the specificity of the bidisperse pore structure: in the simplest case the formation of bidisperse pore structure can be visualized as compaction of primary porous (micro)particles or their aggregates. Spaces between primary particles/agglomerates then form the macropores which run through the whole porous pellet and the size of which can be modified by compacting pressure appreciably. On the other hand the length of narrow mesopores, present already in the primary particles, is commensurable with the primary particle size.

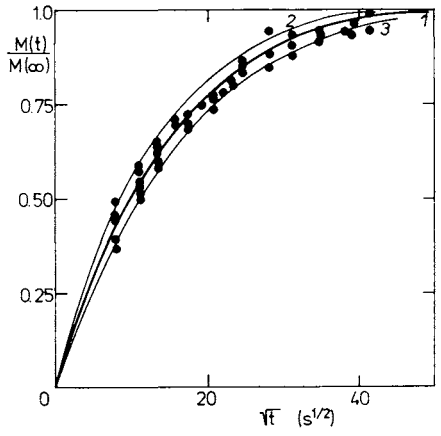

FIG. 5

Diffusion of toluene in binary toluene–cyclohexane for γ-Al_2O_3 compacted at 100 MPa. Points experimental (six independent runs), curve calculated (Eq. (*17*)): *1* $D_{AB} = 6{\cdot}0 \,.\, 10^{-6}$ cm^2/s; *2* $1{\cdot}2D_{AB}$; *3* $0{\cdot}8D_{AB}$

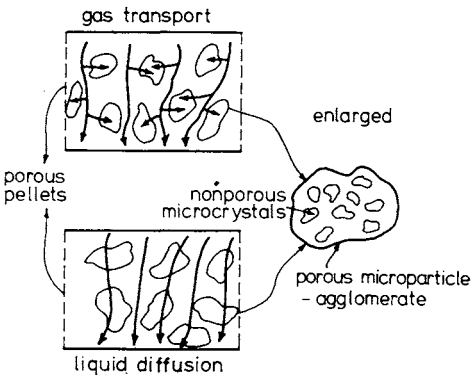

FIG. 6

Schematic representation of gas and liquid transport in bidisperse porous medium

In gas diffusion it is significant that gas diffusion coefficients in narrow pores of primary particles (where the transport is significantly affected by the Knudsen mechanism) are substantially lower then in wide transport pores with bulk molecular diffusion mechanism. Therefore, the mass transport in narrow pores is not running parallel to wide pores and the narrow pores are supplied with diffusing substance from the wide pores (transport in series). This means that the diffusion path lengths are extremely short and the rate of this transport, compared to rate in long transport--pores, is so high that concentration of the diffusing substance in primary particles is identical to concentration in neighbouring transport-pores (see Fig. 6). Thus, the transport resistance is concentrated in wide transport macropores and their mean radius $\langle r \rangle$ and porosity ε_t (appearing in parameter ψ) are characteristic for gas transport.

The situation is different in liquid diffusion: the effective diffusivities are independent of pore size and, thus, the same in wide and in narrow pores. This is the reason for parallel diffusion transport in both pore types (cf. Fig. 6): all pores are now significant for mass transport and the total porosity, ε, appears in the geometric parameter ψ_{liq}.

Tortuosities of γ-Al_2O_3 samples (determined as $q = \varepsilon/\psi_{liq}$ with ψ_{liq} from diffusion measurements with toluene) can serve as an indirect proof of the above argument. For samples compacted at 100, 150, and 250 MPa, the tortuosities are q = 1·8, 2·1, and 2·4, respectively. Tortuosities of this magnitude are commonly found (cf. e.g. Satterfield[11]) and, as expected, increase with increasing compaction pressure. The good agreement of the ratio of macropore volume to the total pore volume ($\varepsilon_{ma}/\varepsilon$) with the ratio of geometric parameters ψ^*/ψ_{liq} is another support for the above conception.

Similar situation is with monodisperse pore structures with wide pore size distributions (e.g. sample ICI 52-1); the marked difference between wide transport pores and narrow pores in primary particles is, howevere, blurred. The transport-pore radius does not differ from the most frequent pore size (maximum on the pore size distribution curve, Fig. 1) as much as in the case of bidisperse porous samples. The low geometric parameter from measurement with gases (ψ^* = 0·09; cf. Table II) witnesses that only a small fraction of pores is decisive for gas transport (on assuming that tortuosity of transport pores q_t = 2, the porosity of transport pores ε_t = 0·18, i.e. only 28% of the total porosity).

For the sample ICI 52-1 the tortuosity $q = \varepsilon/\psi_{liq} = 0{\cdot}66/0{\cdot}45 = 1{\cdot}47$ is again in agreement with the usual results[11].

It is assumed in the applied pore model that there is no interaction between components of the liquid mixture and pore walls, i.e. the same molecular diffusivities $\mathscr{D}_{ij}$ can be used in pore diffusion as in bulk diffusion of liquids in the absence of pore walls. It is obvious that this assumptions is only a crude approximation of the true situation.

CONCLUSIONS

It follows from the comparison of geometric parameters ψ^* and ψ_{liq} (obtained from measurements of combined gas transport and liquid diffusion) of porous samples with bidisperse or wide monodisperse pore structures that transport parameters obtained through evaluation of mass transport of gases cannot be used directly for characterization of liquid diffusion. Similarly, gas transport cannot be predicted with information from liquid phase diffusion. The reason for this is the different role of narrow and wide pores in gas and liquid transport. It follows from considerations based on an simple pore structure model that agreement between parameters ψ^* and ψ_{liq} can be expected for monodisperse porous media with narrow pore size distributions. The difference between wide and narrow pores then disappears and all pores are significant for gas as well as liquid transport. In this case transport characteristics obtained with gases can be used also for liquid transport and vice versa.

We are indebted to Dr J. Linek for densitometric analyses and to Mr R. Pospěch for porosimetric measurements.

REFERENCES

1. Fott P., Petrini G., Schneider P.: Collect. Czech. Chem. Commun. *48*, 215 (1983).
2. Kotter M., Lovera P., Riekert L.: Ber. Bunsenges. Phys. Chem. *80*, 61 (1976).
3. Fott P., Petrini G.: Appl. Catal. *2*, 367 (1982).
4. Valuš J., Schneider P.: Appl. Catal. *1*, 355 (1981).
5. Dreisbach R.: *Physical Properties of Chemical Compounds.* Am. Chem. Soc., Washington 1955.
6. Hála E.: *Fysikální chemie II.* Academia, Praha 1966.
7. Marrero T. R., Mason E. A.: J. Phys. Chem. Ref. Data *1*, 3 (1972).
8. Crank J.: *The Mathematics of Diffusion.* Clarendon Press, London 1975.
9. Sanni A., Hutchison P.: J. Chem. Eng. Data *18*, 317 (1973).
10. Tyn M. T., Calus W. F.: J. Chem. Eng. Data *20*, 106 (1975).
11. Satterfield C. N.: *Mass Transfer in Heterogeneous Catalysis.* MIT Press, Cambridge (Mass.) 1970.

Translated by the author (P.S.).